Anomalous modulus and work function at the interfaces of thin films

U. Harms and R. B. Schwarz
Structure/Property Relations Group, Materials Science Division, Los Alamos National Laboratory, Mail Stop G755, Los Alamos, New Mexico 87545

(Received 17 April 2001; published 6 February 2002)

We use Rayleigh waves and a Kelvin probe to measure the elastic modulus and the work function of thin polycrystalline metallic films prepared by electron beam evaporation. A high-resolution *in situ* measurement of Rayleigh-wave velocities enables us to determine the modulus of the topmost layer of the film (while it is being grown). Using this technique, we can measure the modulus at the interfaces between Ir, Pd, Pt, Ag, and Au. For many metal-pair combinations (e.g., Pt, Ag, or Ir on Pd), each film's modulus equals that of the bulk from the onset of deposition. However, the first couple of nanometers of Pd deposited onto Ir cause an abnormal increase (up to threefold) in the modulus. These same films show an unexpected lower work function. To explain these unusual effects, we present a model based on structural defects in the underlying film. The dependence of modulus and work function on film thickness within a single layer suggests an explanation for previous inconsistent reports of modulus changes in metallic multilayers (i.e., the supermodulus effect).

DOI: 10.1103/PhysRevB.65.085409 PACS number(s): 68.35.Iv, 68.35.Fx, 73.30.+y

I. INTRODUCTION

The plastic and elastic properties of thin-film multilayers have been investigated for many years. In 1970, Koehler[1] proposed that thin-film multilayers could be very strong because it is difficult to activate of Frank-Reed sources inside a confined elastic medium. In 1977, Yang *et al.*[2] reported a large increase in the elastic modulus of thin-film multilayers as the thickness of the individual layers decreased below approximately 10 nm. Called the supermodulus effect, this observation remains controversial because researchers have not reached consensus regarding the effect's origin, magnitude, or even its sign. The effect has been reviewed.[3–5] Most early studies[6] made use of bulge testers to measure the biaxial modulus of the films. Later, more detailed studies suggested that some of the reported modulus enhancements could be caused by experimental artifacts in the testing method.[7]

More recent studies on the elastic properties of films include *in situ* measurements. Some of these studies are based on measuring the speed of surface acoustic waves (Rayleight waves), excited by a laser pulse[8,9] or a piezoelectric transducer.[10,11] In most previous studies, researchers measured the modulus of thin-film multilayers as a function of repetition wavelength. In these studies it is difficult to discern the physical reasons for a modulus change. Studies at a single metal-metal interface have not been conducted previously in part because the techniques employed were not sufficiently sensitive.

In the present work, we use a Rayleigh-wave technique operating at a frequency of approximately 50 MHz. The Rayleigh-wave velocity is measured with a resolution of approximately 1 part in 10^7. With this sensitivity, we can measure *in situ* the modulus of a film of atomic layer thickness as this film is being deposited. We do find an abnormal increase in the modulus of Pd or Pt films deposited onto an Ir film substrate. Measuring the modulus of each film during deposition has definite advantages when we interpret the measurements. To further interpret these results, we also measure the work function of the films.

II. EXPERIMENTAL

The thin films used in this work were prepared by electron-beam evaporation in an ultrahigh vacuum system. The base pressure of the system was approximately 10^{-7} Pa. A quadrupole mass spectrometer attached to the vacuum chamber detected no free oxygen. During evaporation, the pressure was lower than 10^{-4} Pa, with a typical value of 10^{-5} Pa.

The system has two *e*-beam guns, which are operated independently. The evaporation rates are controlled by a pair of quartz-thickness monitors. The distance between the *e*-beam guns and the substrate is large (50 cm) to minimize the direct heating of the substrates during deposition. A mechanical shutter system allows deposition to start with a stable deposition rate.

A. Measurements of Rayleigh-wave velocity

The elastic properties of thin films deposited onto quartz substrates are deduced from changes in the speed of Rayleigh waves. The advantage of this acoustic technique is that most of the wave energy is contained near the topmost region of the substrate and film, within a depth of about one wavelength. We work with Rayleigh waves of approximately 50 MHz. In quartz, these waves have a 60-μm wavelength, much larger than the maximum thickness of our films, which is typically less than 100 nm. In this thickness range we can deduce the elastic properties of the films from a simple linear perturbation theory.[12] With it, we can deposit films in succession onto the same quartz substrate, yet analyze them independently. In addition, by measuring the thickness derivative of the velocity change, we deduce the elastic modulus of the topmost layer being deposited.

The films are deposited through a mask onto the central part of a *X*-cut quartz substrate, as shown in Fig. 1. The substrate has two interdigital transducers (IDT's) for sending and detecting the Rayleigh waves, respectively. Because most metal films are elastically softer than quartz, adding the films slows the Rayleigh wave.

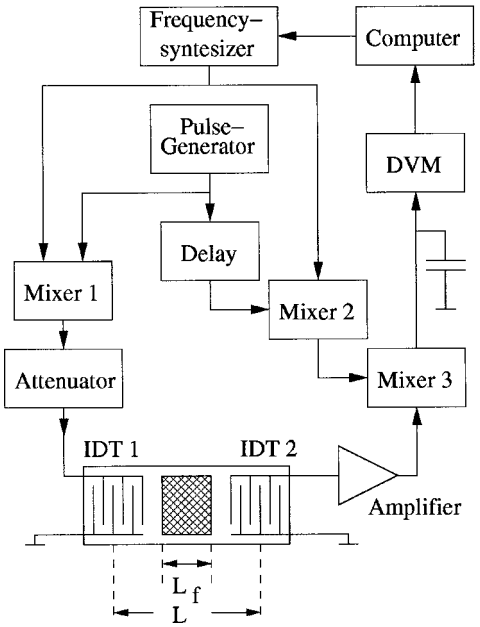

FIG. 1. Schematic of the surface-acoustic-wave transducer and electronics used to measure the elastic properties of thin film. The shaded area on the quartz substrate represents the thin film.

Figure 1 also shows a block diagram of the electronic circuit used to measure the velocity of the Rayleigh waves. We use a pulsed method, which has two advantages: (1) it prevents the direct electrical coupling between the sending and receiving signals and (2) it is insensitive to signals generated by reflections of the Rayleigh wave at the edges of the sample.

The heart of the detection system is a Hewlett-Packard Model 3335*A* frequency synthesizer, whose frequency can be changed via a computer with a resolution of 10^{-3} Hz. For our application, the synthesizer provides a continuous signal at a frequency near 50 MHz. The pulse generator and mixer-1 are used to produce a 50-MHz signal burst, which is applied to IDT-1. IDT-2 detects the Rayleigh wave after it traverses the film. Mixer 3 detects the phase difference between the signal burst received by IDT-2 and the continuous signal provided by the frequency synthesizer; it then produces a dc signal proportional to the cosine of the phase shift. By setting the delay (Fig. 1) equal to the Rayleigh-wave transit time between the IDT's, the signal at IDT-2 is only detected during a narrow time window equal to the width of the signal burst. mixer 3 is of a diode-ring type. The output impedance of this type of mixer is low in the presence of a signal, but it is high otherwise. Consequently, the capacitor stores the voltage generated during the receiving pulse, when the output impedance of mixer 3 is low.

The digital voltmeter reads the dc signal and the resultant data are fed into the computer. The computer then changes the frequency of the synthesizer to keep the phase difference (mixer 3) at a constant value. Because of this negative feedback, changes in the Rayleigh-wave velocity are measured as changes in the carrier frequency, given by

$$\frac{df}{f} = -\frac{dV_R}{V_R}\frac{L_f}{L}, \tag{1}$$

where dV_R/V_R is the relative change in the Rayleigh-wave velocity, L_f is the width of thin film (Fig. 1), and L is the distance between the centers of the IDT's. Typically, we send 2-μs-long pulses every 125 μs.

The detection system has a frequency resolution of approximately 1 Hz, which is equivalent to a Rayleigh-wave-velocity resolution of 1 part in 10^7. The stability of the electronic system is limited principally by thermal drift in the mixers.

We use the change in frequency during evaporation to measure the elastic modulus of a film as it is being grown on the substrate. During deposition, the frequency also changes as a result of (a) an increase in the temperature of the quartz substrate caused by radiation from the evaporation source and (b) the structural relaxation in the film already deposited. For our *X*-cut quartz transducer, an increase in temperature causes a decrease in the Rayleigh-wave velocity, whereas structural relaxation tends to increase the velocity. To determine the effect of temperature, we heat the evaporation source to a temperature just below that needed for film deposition then record the frequency with the shutter closed and open. To determine the effects of structural relaxation, we measure the frequency as a function of time after stopping the deposition. These two effects are quite small when compared to the frequency change caused by the film deposition.

The change in Rayleigh-wave velocity due to a film of thickness Δh deposited onto a quartz substrate is[12]

$$\frac{\Delta V_R}{V_R} = \frac{\Delta h V_R}{4P}\left[\left(\rho - \frac{u_3^3}{V_R^2 D}\right)\nu_x^2 + \rho\nu_y^2 + \left(\rho - \frac{u_5^5}{V_R^2 D}\right)\nu_z^2\right], \tag{2}$$

where ρ is the film density and the quantities ${\nu_x}^2/4P$, ${\nu_y}^2/4P$, and ${\nu_z}^2/4P$ are the normalized particle velocity components at the substrate surface, which are tabulated for many piezoelectric materials and orientations.[12] u_3^3, u_5^5, and D are functions of the elastic compliances of the film. Combining Eqs. (1) and (2), and taking the incremental thickness Δh to the left-hand side, we obtain

$$\frac{1}{f}\frac{df}{dh} = -\frac{L_f}{L}\frac{V_R}{4P}\left[\left(\rho - \frac{u_3^3}{V_R^2 D}\right)\nu_x^2 + \rho\nu_y^2 + \left(\rho - \frac{u_5^5}{V_R^2 D}\right)\nu_z^2\right]. \tag{3}$$

For transversally isotropic films (isotropic in the plane of the film), the u_l^k and D parameters take the simple forms

$$u_3^3 = \frac{(\beta_{11})^2 - (\beta_{13})^2}{\beta_{11}}, \tag{4a}$$

$$u_5^5 = \beta_{55}, \tag{4b}$$

$$D = \frac{\beta_{55}[(\beta_{11})^2 - (\beta_{13})^2]}{\beta_{11}}, \tag{4c}$$

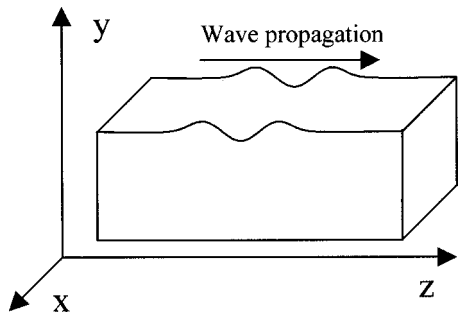

FIG. 2. Coordinate system to define the elastic properties of the thin films.

where β_{ij} are the elastic compliances of the film material, referred to a coordinate system with the y axis normal to the plane of the film, as shown in Fig. 2. Replacing Eqs. (4) into (3), we obtain

$$\frac{1}{f}\frac{df}{dh}=\frac{L_f}{L}\frac{V_R}{4P}\left[\frac{1}{V_R^2}\left(\frac{\nu_x^2}{\beta_{55}}+\frac{\beta_{11}\nu_z^2}{(\beta_{11})^2-(\beta_{13})^2}\right)-\rho(\nu_x^2+\nu_y^2+\nu_z^2)\right]. \tag{5}$$

Equation (5) shows that the modulus measured by the Rayleigh-wave technique is a linear combination of the film's shear modulus $(1/\beta_{55})$ and the flexural modulus $\beta_{11}/[(\beta_{11})^2-(\beta_{13})^2]$. The flexural modulus is the modulus of a plate subjected to a uniform tensile stress along the x direction, which has zero stress in the y direction (normal to the plate) and is constrained to zero strain in the z direction.

It is interesting to compare the two contributions to the measured modulus. For example, using the elastic constants of a (111)-textured Pd film, and the ${\nu_x}^2$ and ${\nu_z}^2$ values for X-cut quartz, tabulated by Auld,[12] we obtain

$$\frac{\nu_x^2}{\beta_{55}}\Big/\frac{\beta_{11}\nu_z^2}{(\beta_{11})^2-(\beta_{13})^2}=0.006, \tag{6}$$

which shows that, to a good approximation, the thin-film modulus measured by the Rayleigh-wave technique is the flexural modulus. This result is a noteworthy difference to Raleigh waves in massive samples, where the velocity of the wave is mainly determined by the out-of-plane shear modulus c_{44}.

Neglecting the ${\nu_x}^2/\beta_{55}$ term in Eq. (5), we obtain

$$M=\frac{\beta_{11}}{(\beta_{11})^2-(\beta_{13})^2}\approx\left(\frac{df}{dh}\right)\left(\frac{L}{L_f}\right)\frac{4PV_R}{f\nu_z^2}+V_R^2\left(\frac{\nu_x^2+\nu_y^2+\nu_z^2}{\nu_z^2}\right)\rho. \tag{7}$$

This equation only applies during film deposition, where df/dh is defined. The first term on the right-hand side of Eq. (7) is usually negative because in most metals the sound velocity is lower than in quartz.

In this work, we are interested in measuring the elastic modulus of metal thin films as they are grown. The measured modulus is proportional to the elastic stored energy in the film. The new, added film need not be continuous to measure a modulus. In a noncontinuous film (e.g., isolated islands), the material will be strained to nearly the same amount everywhere, provided the islands are large in diameter compared to their thickness. The same averaging applies to a rough film. Because the technique measures changes in stiffness, the effect of film roughness vanishes if the roughness does not change during deposition. Even the addition of isolated atoms will cause an increase in stiffness. In such a case, the stiffness change depends on the underlying material (previous thin film) because most of the bonds are to the previous film (not between atoms of the new film). This argument allows us to define a modulus even for submonolayer films.

B. Kelvin probe measurements

The work function of the thin films was measured with a McAllister (Coeur d'Alene, ID 83815) Kelvin probe, Model KP6500. These measurements were conducted between film depositions, without removing the samples from the ultrahigh vacuum. The Kelvin probe measures the potential difference between the film surface and a vibrating electrode, which is parallel to the sample and placed at a separation d. The electrode is maintained at a constant charge so that a periodic change in d produces a periodic change in its potential. For each film, the apparent contact potential is measured as a function of the average distance $\langle d\rangle$ and the measurements are then extrapolated to $\langle d\rangle=0$ to obtain the true contact potential.

Because the Kelvin-probe vibrating electrode is made of stainless steel type 304, the contact potential of the film is measured with respect to this material. The absolute contact potential, or work function, is shifted by 3.6 eV. We obtained this calibration potential shift by measuring the contact potential of elements such as Pd and Ir.

III. EXPERIMENTAL RESULTS

A. Elastic moduli measurements

We used our Rayleigh-wave, *in situ* modulus measurement technique to measure the flexural modulus M of several elemental metallic films and metal-film bilayers. Table I summarizes the results for the elemental films. This table also gives the calculated flexural modulus $M_{\rm cal}$, which was deduced assuming a (111) film texture and averaging the single-crystal elastic compliances.[13] By averaging the compliances, $M_{\rm cal}$ gives a lower bound to the modulus, whereas averaging the stiffnesses gives an upper bound to it. For the current elements of interest, the differences between the lower and upper bounds are only between 1 and 8%.

Figure 3 shows the Rayleigh-wave frequency as a function of time measured during the deposition of Pd onto two different underlying metallic films. In both cases, the Pd deposition rate was kept constant at 0.1 nm/s. As a result, the abscissa also measures the thickness h of the deposited film, as indicated in the upper scale. For Pd on Ag, df/dh is constant from the onset of deposition. The same type of curve was obtained when depositing Pd on Pd. It is not surprising that df/dh is constant for the deposition of Pd onto a

TABLE I. Elastic modulus of elemental thin films, measured by the Rayleigh-wave technique. All films were deposited at a rate of 0.1 nm/s and have thicknesses on the order of 20 nm. s_{11}, s_{12}, and s_{44} are the single-crystal elastic compliances from Refs. 19 and 29. β_{11} and β_{13} are the elastic compliances of a transversely isotropic films with (111) texture, calculated as *s* averages according to Ref. 13. For hexagonal cobalt, $\beta_{11}=s_{11}$ and $\beta_{13}=s_{12}$.

Element	Density g/cm^3	M_{meas} GPa	s_{11} TPa^{-1}	s_{12} TPa^{-1}	s_{44} TPa^{-1}	β_{11} TPa^{-1}	β_{13} TPa^{-1}	M_{calc} GPa
Ag	10.5	27–127[a]	23.1	−9.9	21.7	12.03	−6.21	113
Au	19.3	116	23.4	−10.7	23.8	12.3	−7.0	120
Co	8.84	278	4.75	−2.33		4.75	−2.33	277
Ir	22.4	496	2.28	−0.67	3.9	1.78	−0.503	611
Pd	12.0	187	13.6	−5.95	13.9	7.3	−3.85	190
Pt	21.1	227	7.35	−3.08	13.1	5.41	−2.43	232

[a]The data for Ag has a large scatter.

Pd substrate because, in general, interrupting a film deposition—and continuing to deposit the same element—produces no transient signal in the measured modulus. The fact that df/dh is constant from the onset of Pd deposition onto Ag indicates that there are no abnormal effects at the interface. Palladium and Ag are completely miscible and have a slightly negative heat of mixing in the liquid state of −7 kJ/(mole of atoms).[14] However, a quite different situation is found when depositing Pd onto a thick Ir film. A constant df/dh value is only obtained after the Pd film has reached a thickness of approximately 3 nm. Below that thickness, the frequency has an anomalous, nonlinear, dependence on film thickness (time).

The anomalous modulus effect was always observed when depositing Pd onto Ir. A similar effect, but approximately 3 times smaller, was observed when depositing Pt onto Ir. For several other combinations (Ir on Pd, Ir on Pt, Pd on Ag, Ag on Pd, Pd on Pt, and Pt on Pd), df/dt assumes a constant value from the onset of deposition. For the remainder of this article, we will mainly address the anomalous modulus of Pd deposited onto Ir.

Figure 4 shows df/dt as a function of time (lower abscissa scale) and as a function of film thickness (upper abscissa scale) for Pd deposited onto a thick Ir film at two substrate temperatures. The underlying Ir film was deposited at a rate of 0.1 nm/s and had a thickness in excess of 10 nm. The ordinate scale at the right of the graph gives the film modulus *M*, deduced according to Eq. (7). This scale is only meaningful during film deposition. At the onset of deposition, the film modulus assumes a value of approximately 120 GPa, which is lower than the value expected for a Pd film having (111) texture normal to the film surface (see Table I). The expected value $M_{calc}=190$ GPa, is indicated in Fig. 4 as a dashed line. With increasing film thickness, the film modulus increases, reaching a maximum at a thickness of approximately 0.7 nm. By further increasing the film thickness, the modulus decreases and approaches asymptotically the M_{calc} value. The maximum value reached by the modulus depends on the substrate temperature. For a room-temperature Ir substrate, the excess modulus reaches approximately 220%. Such an increase is quite unexpected.

Diffusion seems to play a role in the magnitude of excess modulus. To estimate the depth of interdiffusion, we investigated the dependence of the peak modulus upon the thickness of the underlying Ir film. Figure 5 shows the maximum

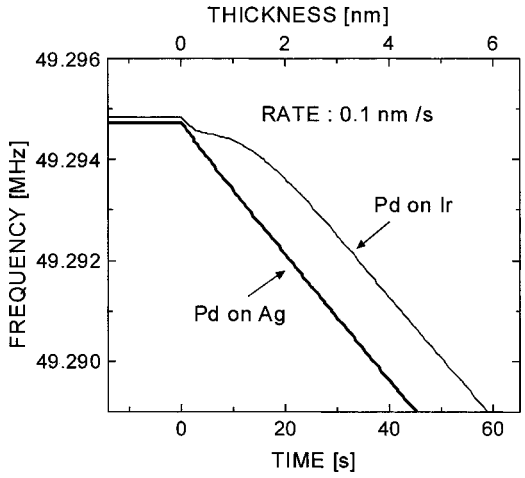

FIG. 3. Rayleigh-wave frequency as a function of time measured during the deposition of Pd onto Ag and Ir.

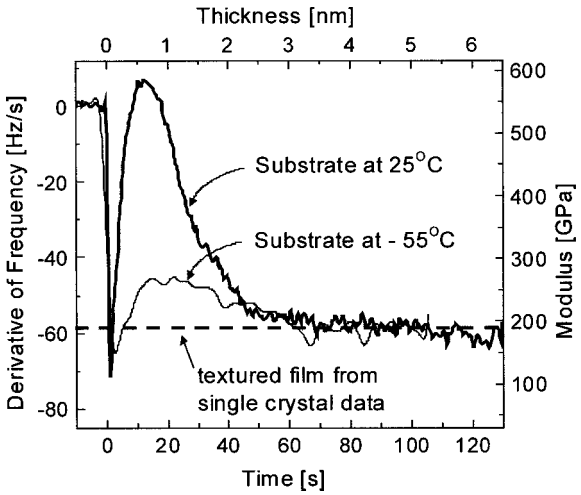

FIG. 4. Time derivative of the frequency df/dt measured during the deposition of Pd onto a thick Ir film. The modulus scale is only valid during the deposition (time>0).

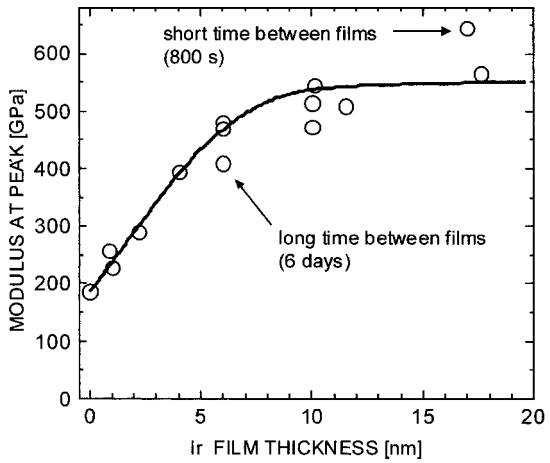

FIG. 5. Maximum value of the modulus of Pd films, deposited onto Ir films, as a function of the Ir film's thickness.

modulus for Pd films deposited onto Ir films of different thicknesses. The Ir and Pd films were deposited in sequence, with a typical delay time between depositions of approximately 2 h. The scattering is partially due to slightly different deposition rates and delay times. The magnitude of the excess-modulus increases with increasing thickness of the Ir underlayer and approaches a saturation value of approximately 550 GPa for an Ir thickness of approximately 15 nm. The arrows in the figure identify two points corresponding to particularly short and long delay times between the depositions of the Ir and Pd films. These points suggest that the excess modulus is smaller when there is a longer delay between the depositions.

Intermixing may be one possible explanation for the anomalous modulus effect at the onset of depositing Pd onto Ir. To further investigate this possibility, we measured the modulus of codeposited Pd-Ir films; the results are shown in Fig. 6. To obtain the alloy films, the deposition rates of Pd and Ir were set at varying constant values. Each alloy film was at least 10 nm thick. Once the deposition rates for each source reached a steady value, the modulus of the codeposited film was more or less constant. Within experimental error, the moduli of the codeposited films follow the linear interpolation between the measured moduli of the pure Pd and Ir films (indicated by the solid circles). What is important to note is that because the modulus follows a linear dependence on composition (Vegard law), the anomalous modulus effect seen in Fig. 4 cannot be explained by simple interdiffusion and mixing at the interface.

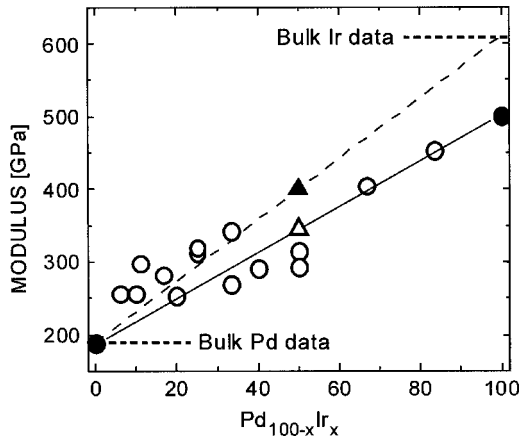

FIG. 6. Flexural modulus of codeposited Pd-Ir films as a function of alloy composition.

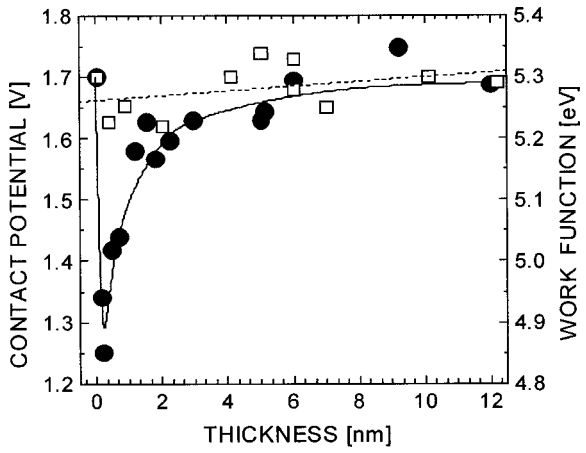

FIG. 7. Thickness dependence of the work function for Pd and Ir films. Open symbols are Ir on Pd and full symbols are Pd on Ir.

The two horizontal, dashed lines in Fig. 6 show the calculated flexural modulus of (111)-textured films of pure Pd and pure Ir (Table I). Although these measured and calculated moduli agree well for the Pd films, they do not for the Ir films. This discrepancy suggests that the Ir films may be defective.

B. Work function measurements

Figure 7 shows the contact potential of (1) a Pd film deposited onto Ir and (2) an Ir film deposited onto Pd, both as a function of film thickness. Each measurement corresponds to a separate film. The measured contact potentials for thick elemental Pd and Ir films merge asymptotically. This occurrence agrees with the literature,[15–18] which quotes work-function values ranging from 5.12 to 5.6 eV for Pd and 5.0 to 5.76 eV for Ir. The fluctuations in the literature values are due to the different measuring methods and the crystallographic surface being tested. The ordinate on the right-hand side gives the work function obtained by shifting our measured contact potential by 3.6 eV. With this shift, the work function for the thick films is 5.3 eV, which corresponds to bulk polycrystalline Pd and Ir.

The work function for Ir deposited onto Pd shows little dependence on film thickness. The dashed line is a least-squares fit to these data. In contrast, the work function for Pd deposited on Ir decreases with increasing thickness, reaching a sharp minimum at a thickness of approximately 0.2 nm. It then increases, approaching asymptotically the work function of bulk Pd. This curve's shape is different from that of the modulus as a function of thickness (Fig. 4). Although both curves reach extreme values at small Pd thickness, notice that the modulus reaches its extreme at approximately 0.7 nm.

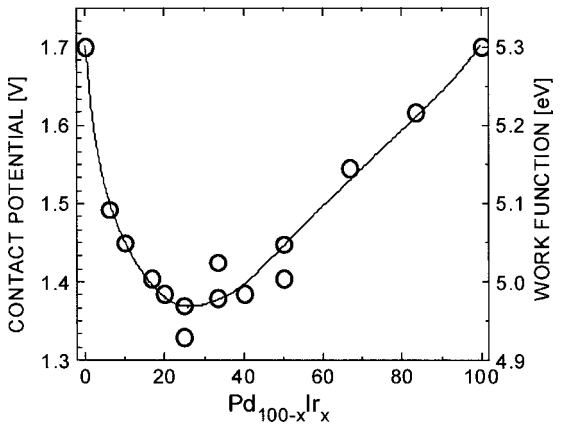

FIG. 8. Work function of codeposited Pd/Ir films. All films are thicker than 10 nm.

Figure 8 shows the work function of codeposited $Pd_{100-x}Ir_x$ films as a function of composition x. Each film had a thickness of at least 10 nm. The work function for the alloy films experiences a minimum at approximately $Pd_{75}Ir_{25}$. The work function at the minimum is approximately 0.35 eV lower than the work functions of elemental Pd and Ir. This behavior contrasts with the results shown in Fig. 6, where the modulus of the codeposited alloy films can be described by a linear combination of the moduli for the elemental films.

C. Film morphology

Atomic force microscopy (AFM) pictures of an Ir film, as well as an Ir film with 0.7-nm Pd deposited on top, look nearly indistinguishable and very smooth. As expected from the small atom-size difference, the Pd grains seem to grow on top of the Ir. Transmission electron microscope (TEM) and AFM measurements show that the grain sizes of the Pd and Ir films both approximately 20-nm thick, are 10 and 8 nm, respectively.

IV. DISCUSSION

Present elastic modulus and work-function measurements have revealed the following seven observations:

(1) The modulus of codeposited Pd-Ir alloy films is a weighted average of the moduli of Pd and Ir films.

(2) The work function of codeposited Pd-Ir alloy films shows a strong negative deviation from the weighted average of the work functions for the elemental films.

(3) Pd and Pt thin films ($\approx$1 nm) deposited onto Ir show a large increase in modulus. The magnitude of the effect decreases when the Pd is deposited on a cooled Ir substrate.

(4) Ir films deposited onto Pd or Pt show no change in elastic modulus, regardless of the Ir film's thickness.

(5) The anomalous modulus change described in (3) is not seen in thin-film couples of Pd/Ag and Pd/Pt.

(6) Depositing a 0.3-nm-thick Pd film onto an Ir substrate lowers the work function by approximately 0.4 eV.

(7) Depositing Ir onto Pd does not change the work function.

The first observation is what would be expected for a single-phase binary alloy with a small heat of mixing as seen, for example, in Ni/Cu, Au/Ni, and Au/Ag alloys.[19] To interpret the second and sixth observations we searched the literature for calculated and measured work functions in alloys and thin films. First-principles calculations for Au-Pt, Cu-Ni, and Ag-Pd solid solutions[20] suggest that the work function of codeposited, binary fcc alloys should follow a linear interpolation between the work functions for the elements. Not only is available data scarce, its interpretation is further complicated because the composition at the surface may differ from that in the bulk. In agreement with these calculations, the work function of bulk Cu-Ni alloys[21] is a linear interpolation of the work functions of pure Cu and Ni.

The work function of indium films deposited onto gold substrates at 80 K (Ref. 22) shows a dependence on film thickness similar to that seen in Fig. 7. The magnitude of this effect is only approximately 0.1 eV, thus making up one-quarter of the effect we measure for Pd films on Ir. The authors[22] attribute the thickness-dependent work function to quantum-size effects that are caused by electronic localization within the thin indium films. Quantum-size effects cannot explain observation two, unless the codeposited Pd-Ir films are phase separated due to, for example, a spinodal decomposition.[23] If such decomposition did occur, then electronic localization could take place within small Pd-rich egions, thus possibly generating a signature similar to that observed in the thin indium films. This model is highly unlikely because it does not explain (a) why the Ir films show no dependence of work function on film thickness and (b) the change in modulus with film thickness.

Two observations suggest that Pd films intermix with Ir substrates (1) there is an observed negative deviation in the work function of Pd deposited onto Ir and (2) the magnitude of this deviation is similar to that measured in the Pd-Ir alloy films (0.45 versus 0.35 eV). Before depositing Pd or Ir, the work function in Fig. 7 has the value 5.3 eV of pure Ir. If during deposition the first monolayers of Pd intermix with the topmost layers of the Ir substrate, the work function would decrease, as suggested by Fig. 8. The work function should reach its minimum value when the composition of the intermixed surface is $Pd_{75}Ir_{25}$ (Fig. 8). With increasing Pd film thickness, the Ir concentration at the (mixed) surface would decrease and the work function would approach that for pure Pd.

It is surprising that the effect on the work function is asymmetric, because no drop in work function is seen on depositing Ir onto Pd. This result suggests that no intermixing takes place at the onset of depositing Ir on Pd. Because intermixing happens when depositing Pd onto Ir but not when depositing Ir on Pd, we can infer that the Ir film is more defective than the Pd film. This difference may be caused by the difference in the homologous deposition temperatures T_{dep}/T_m, where $T_{\mathrm{dep}}\approx 300$ K is the substrate temperature during deposition and T_m is the melting temperature. T_{dep}/T_m equals 0.16 for Pd and 0.11 for Ir.

The lack of intermixing when depositing Ir onto Pd could also explain the normal behavior of the elastic modulus [observation (4)]. The lack of an unusual modulus effect in thin-

film couples of Pd/Ag and Pd/Pt [observation (5)] is easy to explain by either assuming that (a) these elements, deposited sequentially, form atomically sharp interfaces or (b) intermixing does occur but the modulus of the alloyed film equals a linear combination of the moduli of the pure metals.

The observation that the magnitude of the excess modulus (observation three) depends on temperature suggests that the effect involves interdiffusion. However, intermixing alone is not sufficient to explain the excess modulus because the moduli of the codeposited Pd-Ir films are linear combinations of the moduli of pure Pd and pure Ir. To explain observation three, we need to make some further comments on the morphology of the films.

Because the homologous deposition temperature for the Ir films is so low, we expect these films to be highly defective, containing a large density of point defects, lattice defects, and voids. Could these defects be responsible for the low modulus of our as-deposited Ir films ($M_{\mathrm{meas}}/M_{\mathrm{calc}}=0.81$; see Table I)? To proceed, we must examine the dependence of the modulus on size and defect density. Gleiter *et al.*[24,25] studied the elastic properties of nanosized crystalline solids obtained by densifying nanoparticles prepared by gas condensation. The Young's modulus of Pd samples prepared this way was 71% of that for bulk polycrystalline Pd. The large decrease of the modulus was attributed to the large number of grain boundaries and triple points in the material. However, it should be noted that the density of these samples was 85% of that for bulk Pd. Huang and Spaepen[26] measured the static Young's modulus in thin films of Cu, Ag, and Al, all of which were prepared by vacuum deposition. They found that the static modulus was approximately 80% of that calculated from bulk elastic constants, taking into account the film texture. The modulus decrement was attributed to incomplete cohesion (microcracking) at the grain boundaries. In addition, their modulus could have been reduced by grain boundary sliding.[27] Shen *et al.*[28] used a nanoindentation technique to measure the modulus of nanocrystalline Fe, Cu, Ni, and Cu-Ni alloy. The modulus in these fully dense materials was much closer to the single-crystal values. Their measurements in small-grained Fe show that the decrease in Young's modulus becomes noticeable as the grain size decreases below approximately 15 nm. According to these results, the Young's modulus of a Fe film having 10-nm grains should be approximately 5% lower than that of large-crystal Fe. These three studies[24,26,28] show that nanocrystalline materials have lower elastic moduli than bulk crystals. However, these studies do not allow us to predict the modulus of our 10-nm grain size Ir films.

Based on the foregoing, we propose the following model: It is highly probable that the present nanocrystalline Ir films have a large density of atom-size voids, which cannot be resolved by techniques such as TEM and AFM. These voids reduce the film modulus. When Pd is deposited onto the defective Ir film, Pd atoms diffuse into the Ir film to occupy defective sites near dislocations, grain boundaries, and voids. The diffusion stiffens the elastically softer parts of the Ir film, causing an increase in the Ir film's modulus. This increase in turn causes a large *apparent* increase in the modulus of the added Pd film. Figure 9 shows a schematic of the model. The essence of this model is that the modulus increase observed on depositing Pd onto Ir is not caused by a stiff Pd film, but rather is caused by the repairing effect that Pd has on the topmost Ir layer.

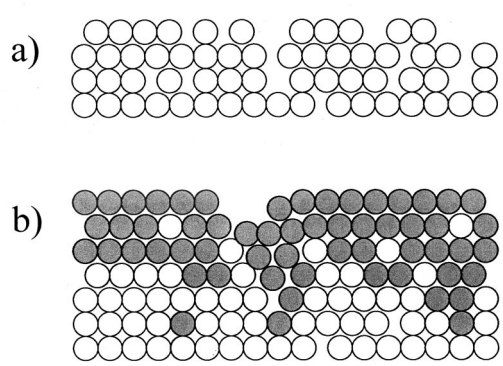

FIG. 9. Illustration of model for Pd film on Ir film: (a) defective Ir film and (b) Pd film on top of Ir, repairing the Ir film.

The data in Fig. 5 suggest that Pd diffuses into the Ir underlayer up to a depth of approximately 7 nm. The area defined by the 25 °C curve and the dashed line in Fig. 4 equals 500 GPa×nm. This value is the integrated excess modulus. Dividing this value by the 7-nm depth gives an average modulus increase of approximately 70 GPa. This value compares favorably with the difference between the measured modulus for the as-deposited nanocrystalline Ir film and the known modulus of large-grain polycrystalline Ir (see Table I).

Conditions that favor this type of excess modulus are film combinations of high- and low-melting-point materials. In addition, the high-melting-point material should have a high modulus. However, these two properties usually come together. If the high-melting-point film is defective, part of the low-melting-point film deposited on top would diffuse into the former, patching up a fraction of the defects. Figure 6 can be used to illustrate the magnitude of the effect. The modulus of an equimolar multilayer of thick Pd and Ir films (each thicker than 20 nm) should have a modulus of approximately 350 GPa, as indicated by the open triangle located on the solid line joining the moduli for films of Pd and Ir. This is because in the multilayer of thick films, the Ir films are defective and thus have a relatively low modulus. In contrast, the modulus of an equimolar multilayer of thin Pd and Ir films, each having a thickness of approximately 7 nm (or less), will have a modulus of approximately 400 GPa, as indicated by the solid triangle located on the dashed line joining the moduli of bulk Pd and bulk Ir. This is because in the multilayer of thin films, each Ir film has been ''repaired'' by Pd atoms diffusing from the following Pd film. This 50-GPa modulus increment could be interpreted as a supermodulus effect.

ACKNOWLEDGMENTS

This work was supported by the U.S. Department of Energy, Office of Basic Energy Sciences, Division of Materials Sciences. The authors thank Dr. M. E. Hawley for help with the AFM observations.

[1] J. S. Koehler, Phys. Rev. B **2**, 547 (1970).
[2] W. M. C. Yang, T. Tsakalakos, and J. E. Hilliard, J. Appl. Phys. **48**, 876 (1977).
[3] B. M. Davis, D. N. Seidman, A. Moreau, J. B. Ketterson, J. Mattson, and M. B. Grimsditch, Phys. Rev. B **43**, 9304 (1991).
[4] A. Fartash, E. E. Fullerton, I. K. Schuller, S. E. Bobbin, J. W. Wagner, R. C. Cammarata, S. Kumar, and M. Grimsditch, Phys. Rev. B **44**, 13 760 (1991).
[5] R. C. Cammarata, Thin Solid Films **240**, 82 (1994).
[6] T. Tsakalakos and J. E. Hilliard, J. Appl. Phys. **54**, 734 (1983).
[7] S. P. Baker and W. D. Nix, J. Mater. Res. **9**, 3145 (1994).
[8] S. E. Bobbin, J. W. Wagner, and R. C. Cammarata, Appl. Phys. Lett. **59**, 1544 (1991).
[9] D. Schneider, Th. Witke, Th. Schwarz, B. Schoeneich, and B. Schultrich, Surf. Coat. Technol. **126**, 136 (2000).
[10] R. Danner, R. P. Huebner, C. S. L. Chun, M. Grimsditch, and I. K. Schuller, Phys. Rev. B **33**, 3696 (1986).
[11] J. B. Rubin and R. B. Schwarz, Phys. Rev. B **50**, 795 (1994).
[12] B. A. Auld, *Acoustic Fields and Waves in Solids* (Krieger, Malabar, FL), Volume 2, Chapter 12.
[13] D. Baral, J. E. Hilliard, J. B. Ketterson, and K. Miyano, J. Appl. Phys. **53**, 3552 (1982).
[14] F. R. de Boer, R. Boom, W. C. M. Mattens, A. R. Miedema, and A. K. Niessen, *Cohesion in Metals* (North Holland, Amsterdam, 1989).
[15] R. G. Wilson, J. Appl. Phys. **37**, 3170 (1966).
[16] B. E. Nieuwenhuys, R. Bouwman, and W. M. H. Sachtler, Thin Solid Films **21**, 51 (1974).
[17] R. W. Strayer, W. Mackie, and L. W. Swanson, Surf. Sci. **34**, 225 (1973).
[18] J. E. Demuth, Chem. Phys. Lett. **45**, 12 (1977).
[19] G. Simmons and H. Wang, *Single Crystal Elastic Constants and Calculated Aggregate Properties* (M.I.T. Press, Cambridge, 1971).
[20] I. A. Abrikosov and H. L. Skriver, Phys. Rev. B **47**, 16 532 (1993).
[21] Y. Takasu, H. Konno, and T. Yamashina, Surf. Sci. **45**, 321 (1974).
[22] C. Marliere, Vacuum **41**, 1192 (1990).
[23] de Boer *et al.* (Ref. 14) predicts an equimolar fcc mixture of Pd and Ir has a heat of mixing of $+9$ kJ (mole atoms)$^{-1}$. The Pd-Ir equilibrium phase diagram predicts a spinoldal decomposition below approximately 1480 °C.
[24] H. E. Schaefer, R. Wurschum, R. Birringer, and H. Gleiter, J. Less-Common Met. **140**, 161 (1988).
[25] D. Korn, A. Morsch, R. Birringer, W. Arnold, and H. Gleiter, J. Phys. Colloq. **49**, 769 (1988).
[26] H. Huang and F. Spaepen, Acta Mater. **48**, 3261 (2000).
[27] H. G. Bohn, M. Prieler, C. M. Su, H. Trinkhaus, and W. Schilling, J. Phys. Chem. Solids **55**, 1157 (1994).
[28] T. D. Shen, C. C. Koch, T. Y. Tsui, and G. M. Pharr, J. Mater. Res. **10**, 2892 (1995).
[29] *Landolt-Bornstein: Zahlenwerte und Funktionen aus Physik, Chemie, Astronomie, Geophysik und Technik* edited by K. H. Hellwege and A. M. Hellwege (Springer, Berlin, 1969), Vol. III/2.